Plasmonics
https://doi.org/10.1007/s11468-024-02683-w

RESEARCH

SPR-Based Fiber Optic Sensor for the Development of Internet of Things (IoT) Technologies

Mst Nargis Aktar[1] · Nilanjana Basak[1] · Shuvo Biswas[1] · Hasan Abdullah[1,2] · Muhammad Shahin Uddin[1]

Received: 22 October 2024 / Accepted: 22 November 2024

Abstract

Photonic crystal fiber (PCF) is a crucial component of optical fiber. Today, PCF has sparked widespread interest because of its potential in sensor systems, photonic devices, and communication. However, the features of technologies are updating day by day, and to keep up with the latest features, optical fiber sensors are a key issue for the Internet of Things (IoT) technologies. The primary goal of the offered project is to design an optical sensor for IoT-compatible devices with maximum sensitivity and minimum loss. Therefore, this project presents a unique circular-shaped PCF sensor based on surface plasmon resonance (SPR) for evaluating analyte refractive index (RI). With the utilization of the finite element approach, the sensing capabilities of the proposed structure have been examined via numerical simulations incorporating an iterative optimization. However, in this configuration, several capillaries are collected and conducted to yield a circular-shaped silica structure, and the flattened layer is then coated with a gold (Au) material. The gold material obtains the SPR pulse in the PCF's broadcast spectrum. In this structure, the operating wavelength range of 0.94–0.62 µm yields efficient results. All the parameters are numerically simulated for the analyte, with RI = 1.34–1.37. After the simulation and formal analysis, the offered sensor gives the highest wavelength sensitivity response of 18,403.59 nm/RIU and a minimum loss peak of 193.87 dB/cm. We believe the structural design can also be an appropriate candidate for biological and organic detection, as well as other IoT-based applications.

Keywords Photonic crystal fiber · Internet of Things · Surface plasmon resonance · Perfectly match layer · Sensitivity · Sensor

Introduction

Surface plasmon resonance (SPR)-based sensors have received varied attention from researchers currently due to their extremely flexible features and vast application in a range of practical domains. SPR-based sensors are utilized in a range of real-world tasks, i.e., gas detection [1], water testing [2], organic molecule sensing, food quality maintenance, clinical trials, disease identification, bioimaging, real-time observation, biosensing, environment monitoring, and glucose monitoring [3–7]. Researchers have developed several beneficial applications on the basis of SPR sensors [3–6], terahertz sensors [8], and optical sensors [9–14] for the advancement of existing technology. Among these sensors, Ritchie et al. (1950) coined SPR analytically at first [15]. After a long time, Liedberg et al. (1983) coined SPR [16], based on the idea of prism coupling. These sensors typically use conventional prism coupling geometry. Prisms are employed to move the light to the layer of metal boundary, while p-polarized or transverse magnetic light is generated on the dielectric or

✉ Mst Nargis Aktar
nargis_ict@mbstu.ac.bd

✉ Shuvo Biswas
shuvo.ict13@gmail.com

Nilanjana Basak
nilanjanabasak96@gmail.com

Hasan Abdullah
hasanabdullah989@gmail.com

Muhammad Shahin Uddin
shahin.mbstu@gmail.com

[1] Department of Information and Communication Technology, Mawlana Bhashani Science and Technology University, Tangail 1902, Bangladesh

[2] Department of Computer Science and Engineering, Bangladesh Army International University of Science and Technology, Cumilla, Bangladesh

Published online: 02 December 2024

metal surface. This situation appears when light impacts the top metal layer and the scattered electrons capture it, resulting in a surface plasmon wave. People commonly use prisms to trigger surface plasmons. However, prism-based SPR sensor technology has a few pitfalls, like a heavy device containing a variety of mechanical and optical parts, making it unsuitable for distant sensing technologies [17]. The OF (optical fiber) is utilized alternatively to the prism to reduce the allusive pitfall. SPR-based OF sensors are primarily utilized to minimize the computational requirements and the overall size of detectors. At first, a SPR-based OF sensor was proposed by R.C. Jorgenson (1993) [2], where a gold (Au) coating was implemented to expose the plasmon effect [2]. PCF has achieved popularity because of its several alluring benefits, i.e., optimal confinement, SMP (single mode propagation), and precise birefringence [5, 6, 15–18]. These benefits allow for the beneficial adjustment of an evanescent field (EF) in the fiber. The EF is responsible for the fiber's optimal sensitivity results. The recent development of plasmonic tools, the outstanding surface-to-volume proportion, and extensive optical strengths serve as ideal candidates for sensing applications using OF detectors and efficient coating components [19, 20]. However, SPR-based detectors exhibit greater sensitivity than non-SPR fiber-based detectors. It provides a lower resonant peak compared to OF sensors [21–23]. PCF-based sensors additionally offer an adaptable architecture. Gold is used to simulate most of the SPR-based sensors [5, 24, 25]. Motivated by the above benefits, in this improved structure, we focus on a gold layer due to its chemical robustness, which exhibits broader oscillations in appeal wavelengths [5]. For the purpose of optimizing the reliability of SPR-based PCF sensors, the researchers have attempted to formulate innovative structures during the past few years. They have attained optimal sensitivity to substantial confinement loss (CL) through their unique approaches. They have also effectively boosted the reliability of SPR-based PCF sensors. In prior decades, Rifat et al. [22] published an article on PCF-based SPR in which a gold (Au) material (thickness 40 nm) was coated utilizing the fused silica (FS) and found a maximum WS (wavelength sensitivity) of 1000 nm/RIU. However, they suggested an SPR biosensor on the basis of a polymer PCF-coated configuration. Dash et al. [22] enhanced the AS (amplitude sensitivity) to 80 RIU^{-1} and the maximum WS to 2000 nm/RIU. In the past, the manuscript [26] improved the maximum WS to 2200 nm/RIU and the AS to 266 RIU^{-1} over [22] by putting forward a new concept for useful sensing devices. Chakma et al. (2018) presented a manuscript [2] that enhanced the maximum WS to 9000 nm/RIU and the AS to 318 RIU^{-1}, compared to [26]. Their proposed structure exhibits better performance than [2]. However, recently, Azman et al. [27] (2024) published an internal PCF model with dual modes, including a selective metal coating around the air holes. Though they proposed a novel method, their method makes the fabrication process more complex and time-consuming. Their offered sensor shows a low WS of 11,000 nm/RIU. In another study, Mahfuz et al. (2020) [28] offered an external PCF model that exhibits a very high WS of 28,000 nm/RIU. Recently, in 2020 [29], Srivastava et al. offered an external micro-channel SPR model with a D shape that gives a very high WS of 67,000 nm/RIU. In another article, Haque et al. (2021) [30] presented an intricate SPR sensor with a D shape in which a WS of 216,000 nm/RIU is achieved. This is an excellent outcome, but the fabrication of the D-shaped model is highly complicated and less effective due to its precise surface area. Again, Sharif and colleagues (2023) [31] presented a circular SPR model for external sensing of metals that explores the WS of 13,800 nm/RIU. In this manuscript, a straightforward circular PCF-based sensor has been presented that is composed of two convergent silica layers, where a thin metal named gold (Au) is added on the topmost layer of the PCF model. The presented configuration was developed to gain high sensing performance and high coupling sensitivity, such as sensor resolution and AS (amplitude sensitivity). Several gold (Au) thicknesses, the area of the perfectly matched layer (PML), the diameter (D), and the pitch of the circle have been evaluated to determine the precise sensing performance for the suggested configuration. From analyzing the simulated results, we have noticed that the presented configuration is able to generate higher performance for sensing the IoT-compatible devices from the above-mentioned papers.

The novelty of this work is to design a circular-shaped PCF sensor that integrates SPR for ultra-sensitive RI detection. Unlike traditional fiber sensors, the proposed structure leverages a unique combination of a silica-based capillary array and a gold (Au) coating, which significantly enhances the sensor's sensitivity and reduces loss. This high sensitivity with a broad operating wavelength range makes the suggested sensor more accurate for detecting subtle environmental or biological changes, which is essential for IoT-based systems. In the context of the IoT, where real-time monitoring, low-power consumption, and rapid data processing are crucial, this PCF-based sensor can be integrated into a wide array of smart devices such as environmental sensors, medical diagnostics, and wearable technology. Thus, this work introduces a novel sensor architecture that can play a significant part in the advancement of next-generation IoT technologies, particularly in applications where high precision and low energy are needed.

Design Methodology

The configuration of a sensor greatly influences its sensing capacity. The overall architectural shape, such as the location and number of circular air holes (CAH), determines the guiding features and sensing capacity. However, in this

manuscript, a unique SPR-based sensor is suggested with CAH and a gold (Au) coating layer is applied for external sensing. We attached a PML to this sensor to measure its performance. The main function of this PML layer is to minimize undesired nonphysical radiation. Figure 1 illustrates the offered sensor. As an exterior material, this sensor utilizes a fused silica (FS) layer with a 0.4-µm radius. Then, a 40-nm-thick gold (Au) coating is employed on top of this FS to generate plasmonic outcomes. A circular channel with a width of 0.56 µm is covered with the liquid analyte. Finally, circular PMLs are applied around the sensor borders. In the cladding layer (CL), air holes with ranges from 0.20 to 0.30 µm in radius are provided in a circular manner around the analyte circle. In the outer part of the CL, a circular-formed PML with 0.5-µm-thick and scattering boundary conditions is employed to absorb scattered radiation.

Despite the fact that the proposed work is simulation based, Fig. 2 represents a simplified block diagram of the offered sensor. The optical signal is transmitted through a SMF (single-mode fiber) by applying a light source (monochromatic and broadband). A connection is established between the PCF and the light using the higher-level SMF. Conversely, another connection is established between the PCF and the optical spectrum analyzer using the lower-level SMF. Additionally, a photodetector, or OSA, has been used to uniquely identify the transferred light. Finally, the simulated results were recorded using a high-configuration computer.

Numerical Investigation

This portion presents a numerical investigation of propagation features in fundamental modes. In OFC, refractive index (RI) is a dimensionless number that indicates how light passes through a medium. In this article, we used FS as the base material. We calculate the RI of FS using Sellmeier's formula in Eq. (1) [32].

$$n(\lambda) = \sqrt{1 + \frac{P_1\lambda^2}{\lambda^2 - Q_1} + \frac{P_2\lambda^2}{\lambda^2 - Q_2} + \frac{P_3\lambda^2}{\lambda^2 - Q_3}} \tag{1}$$

where n represents the RI of FS, λ is the wavelength (µm), $P_1 = 0.696166300$, $Q_1 = 4.67914826 \times 10^{-3}$ µm^2, $P_2 = 0.407942600$, $Q_2 = 1.35120631 \times 10^{-2}$ µm^2, $Q_3 = 97.9340025$ µm^2, and $P_3 = 0.897479400$.

To develop this novel structure, we chose gold (Au) as a plasmonic material because of its low loss pattern in the near-infrared spectrum. We evaluate the permittivity of Au based on the Lorentz–Drude framework [33], and the formula for this permittivity is given in Eq. (2).

$$\varepsilon_{\mathrm{Au}} = \varepsilon_{\infty} - \frac{\omega_D^2}{\omega\left(\omega + j\gamma_D\right)} - \frac{\Delta\varepsilon.\Omega_L^2}{(\omega^2 - \Omega_L^2) + j\Gamma_L\omega} \tag{2}$$

where $\varepsilon_{\mathrm{Au}}$ represents Au permittivity, permittivity represents ε_{∞} at high frequency, plasma frequency represents ω_D, decaying frequency represents Υ_D, and angular

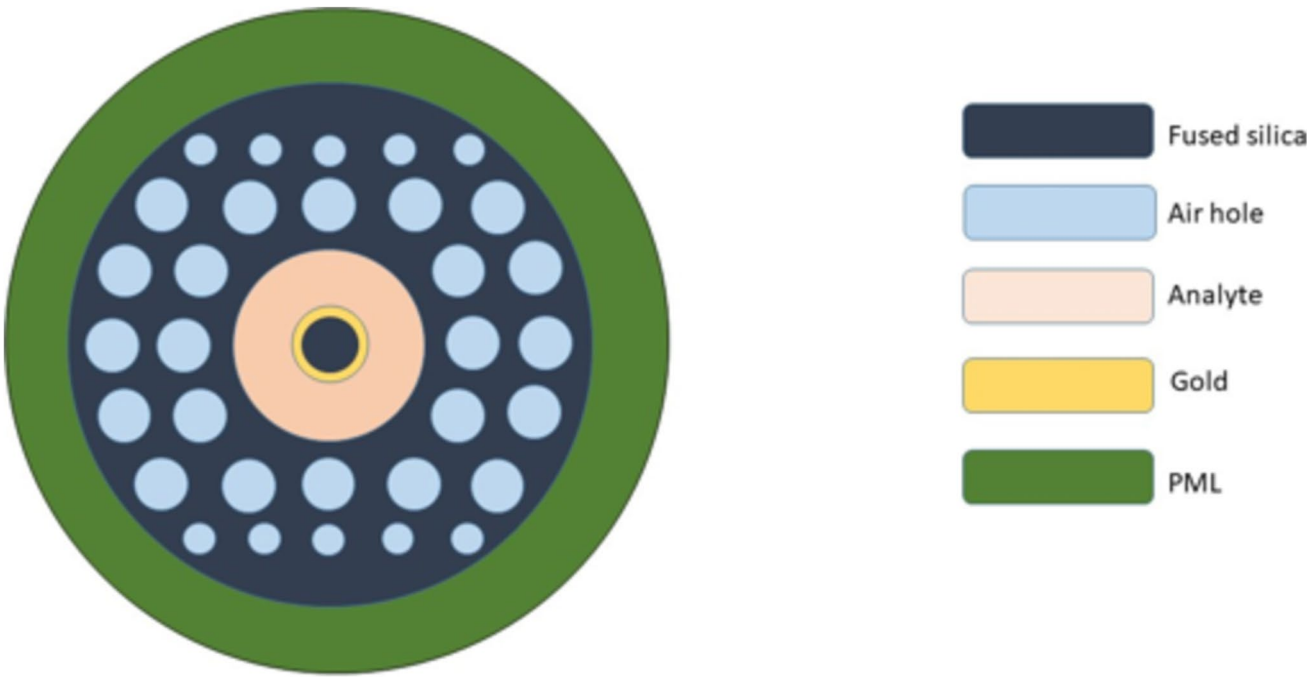

Fig. 1 Cross-sectional representation of the offered sensor

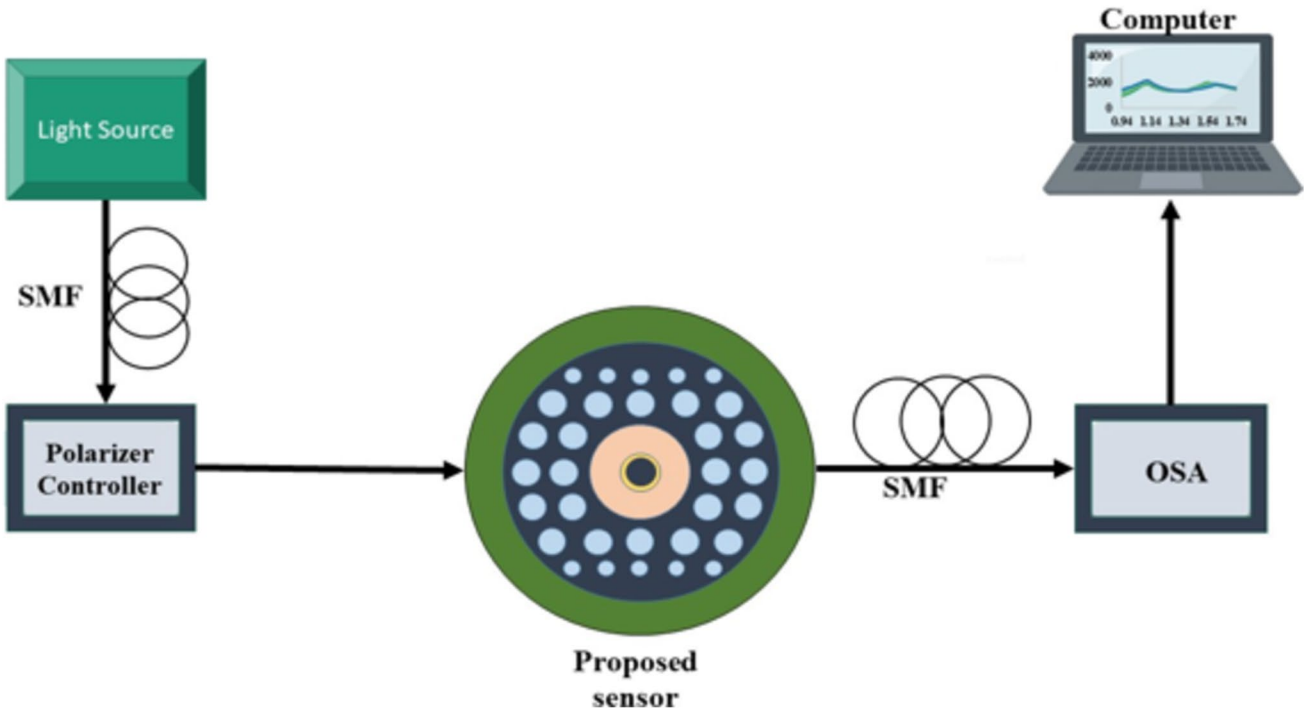

Fig. 2 Block diagram of the offered work

frequency represents ω. Again, $\omega = 2\pi c/\lambda$, $\varepsilon_\infty = 5.9673$, c represents light velocity (vacuum), $\Upsilon_D/2\pi = 15.92$ THz, weighting factor $\Delta\varepsilon = 1.09$, and $\omega_D/2\pi = 2113.6$ THz. Additionally, the oscillator strength is $\Omega_L/2\pi = 650.07$ THz, and the spectral width of Lorentz is $\Gamma_L/2\pi = 104.86$ THz.

Different kinds of losses could occur during the propagation of light. One of them is confinement loss (CL). When a mode is compressed into a limited space, it partially propagates the outer surface of the fiber and is encountered in the CL. The formula for the CL with parameters is given in Eq. (3) [24]:

$$\alpha(\mathrm{dB/cm}) = 8.686 \times \frac{2\pi}{\lambda} \times \mathrm{Im}[n_{\mathrm{eff}}] \times 10^4 \tag{3}$$

Here, α is the confinement loss (dB/m), λ is the operating wavelength (μm), and $\mathrm{Im}[n_{\mathrm{eff}}]$ is the imaginary mode of the effective RI.

WS is the variation in peak wavelength related to the difference in RI. Equation (4) provides the WS response formula derived from the CL spectrum [34].

$$S\left(\frac{\mathrm{nm}}{\mathrm{RIU}}\right) = \frac{\Delta\lambda_{\mathrm{peak}}}{\Delta n} \tag{4}$$

where Δn represents the variance of the related RI and $\Delta\lambda_{\mathrm{peak}}$ is the resonance peak variance.

Birefringence (Bi) indicates the RI variance between X- and Y-polarization [34], and it can be estimated leveraging Eq. (5).

$$B_i = n_x - n_y \tag{5}$$

Here, n_x and n_y indicate the RI of the fundamental mode at X- and Y-polarizations, respectively.

Another crucial performance measurement parameter of the sensor is coupling length (CPL). It is measured with the help of BI, as CPL is inversely correlated to BI [35]. Equation (6) represents the formula for CPL.

$$L_C(\mu\mathrm{m}) = \frac{\lambda}{2B_i} \tag{6}$$

The output power (OP) of a sensor spectrum is measured based on its BI and CPL [35]. The formula for the OP spectrum to obtain fiber efficiency is given in Eq. (7).

$$P_o(\mathrm{dB/m}) = \sin^2((B_i\pi l)/\lambda) \tag{7}$$

where l represents the fiber length.

Another crucial parameter, the transmission spectrum (TS), is utilized to quantify the sensor's efficiency by computing the data transmittance rate [35]. The formula for transmittance is given in Eq. (8).

$$T(\mathrm{dB}) = 10\log_{10}(P_o/P_i) \tag{8}$$

where T represents the transmittance (dB). P_i and P_o represent the maximum input and output powers, respectively.

Result Analysis and Discussion

The evanescent field (EF) needs to be adjusted in a way that allows it to simply interface with the electrons in the metallic layer so that it achieves improved sensing performance. Our offered sensor's EM field dispersal is for both x-pol (*x*-polarized light) and y-pol (*y*-polarized light). From Fig. 3a, b, we see the narrow confinement of light, which means low CL. Figure 3c, d shows the SPP mode, which indicates good guiding characteristics because of the exact location of circular air holes. Suitable EF-metal surface contact generates a reliable SPR mode-core mode coupling.

Figure 4a, b exhibits the CL spectrum of the suggested sensor for x-pol and y-pol, respectively. We select just two peaks to evaluate the CL spectrum. From Fig. 4a, we clearly see that these two peaks also rise when the analyte RI rises. Conversely, in Fig. 4b, these two peaks of the RI analytes have a distinct relationship. From Fig. 4b, we also see that for the first peak, the amplitude of the LC (loss curve) rises when the RI rises. Conversely, as the RI of the second peak increases, the amplitude of the LC diminishes. The WS of 12,605.65, 18,403.59, 22,919.85, and 6712.853 nm/RIU for x-pol and 15,248.513, 15,896.46657, 15,904.437, and 5004.148 nm/RIU for y-pol are obtained for RI = 1.34–1.37, respectively.

Throughout the entire process, the wavelength fluctuates between 1.12 and 1.42 µm since the RI rises from 1.34 to 1.37. Figure 5 shows the changes with regard to wavelength. Figure 5 also shows that the RI variation grows gradually as the wavelength rises. When the RI hits 1.37, then the highest BI is obtained. This peak in BI is significant, as it suggests that the material could serve as a promising candidate for SPR-based sensor applications, where high BI values can enhance sensitivity and performance. Since birefringence offers important information on the anisotropic characteristics of the material, which influence how light travels through it, it is included in this analysis. The material's optical response is mostly determined by structural stresses, compositional inhomogeneities, and internal molecular alignment, all of which can be revealed via birefringence. Birefringence evaluation helps us comprehend how the structure of the material affects its RI in different scenarios, which is crucial for applications like SPR-based sensing. This highest value of BI makes it a potential candidate for SPR-based sensor developments.

Figure 6 exhibits the CL of the proposed structure across a RI of 1.34–1.37. As shown in the figure, the CL increases with wavelength, indicating an inverse relationship between the two parameters. We also observe that there exists a correlation among these RI values, such as a greater RI value demonstrating a lower CL. The nature of the analyte interactions is responsible for this behavior; shorter analytes generally show a more noticeable PL response and a lower BI. The greater CL indicates extended filling time, larger analyte quantities, and extended filling length within the structure [36]. A key consideration in assessing the effectiveness and strength of mode coupling is CL, which is the distance over which energy is exchanged between modes in coupled waveguides or fibers. To give an extensive understanding of the interaction between guided modes inside the optical structure, the CL is incorporated into this analysis.

Figure 7 demonstrates the TS of the proposed structure for RI = 1.34–1.37. The values of the power spectrum change from 0 to 1 based on the sinusoidal wave. The greater RI value has a larger wave than the smaller RI value. However, RI = 1.34 was the most forward, whereas RI = 1.35 was the most backward. The transmission spectrum (TS) shown in Fig. 7 represents the interaction between the guided light in the PCF and the surface plasmon wave. The dips in the TS correspond to the resonance

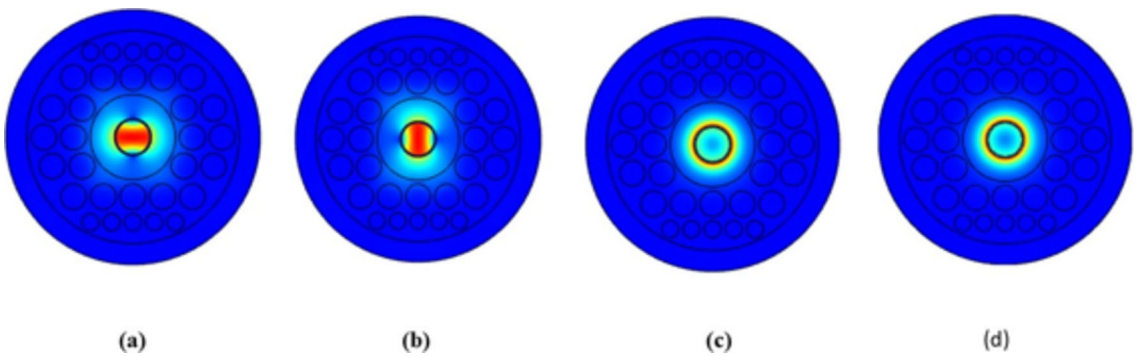

Fig. 3 Field distribution of **a** x-pol core mode, **b** y-pol core mode, **c** x-pol SPP mode, and **d** y-pol SPP mode

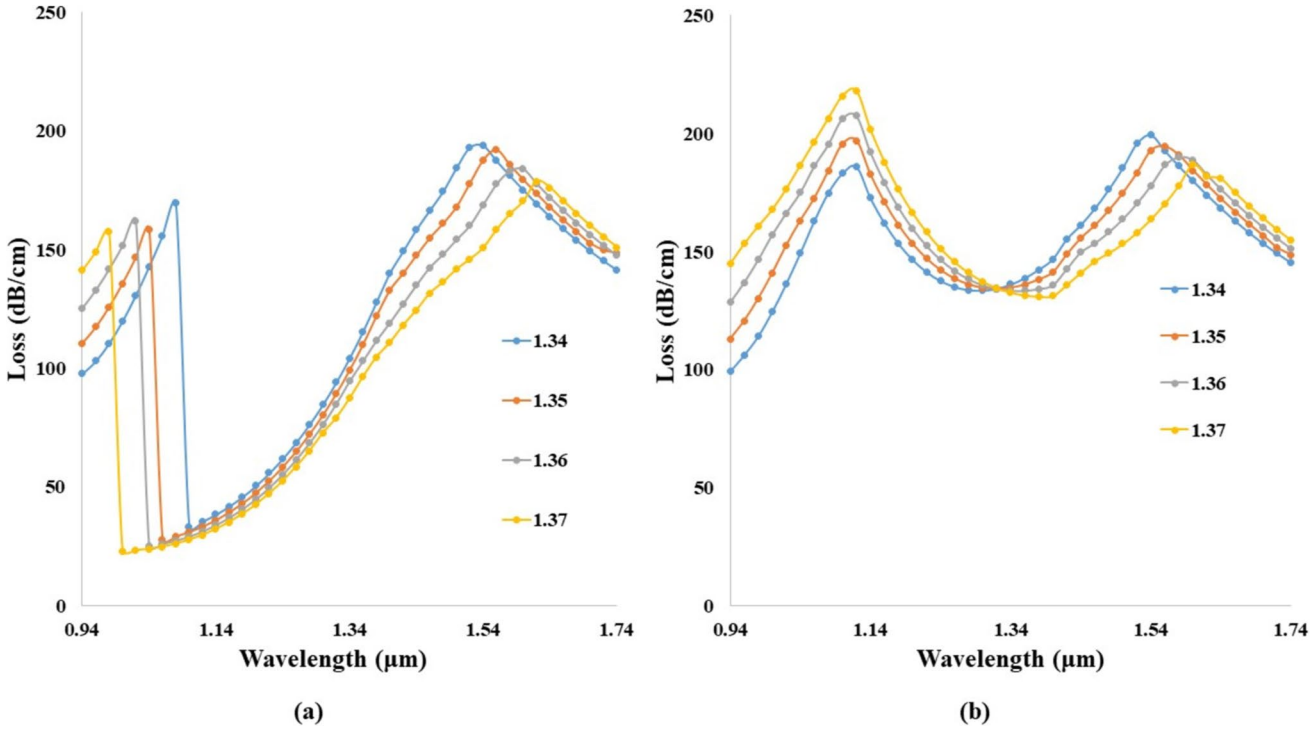

Fig. 4 The confinement loss curves while analyte RI is 1.35, 1.36, 1.37, and 1.38 for **a** x-pol and **b** y-pol

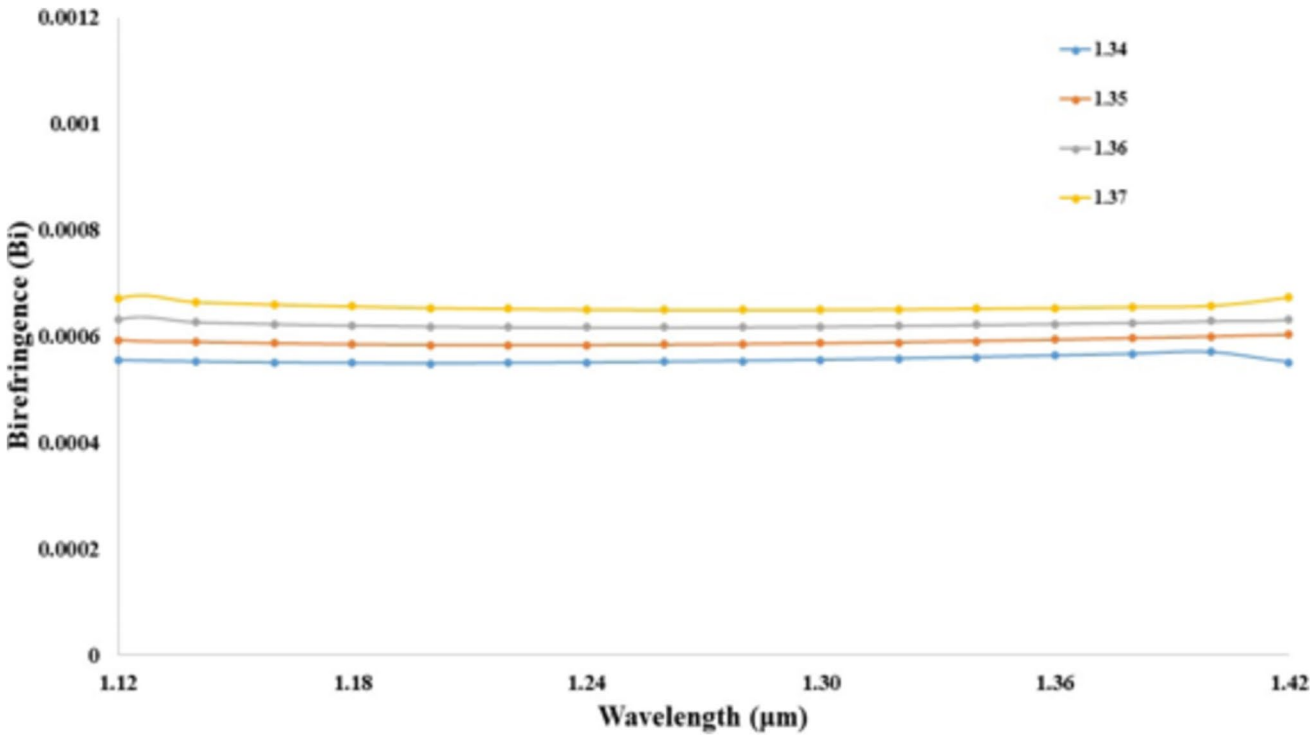

Fig. 5 Birefringence vs. wavelength curve

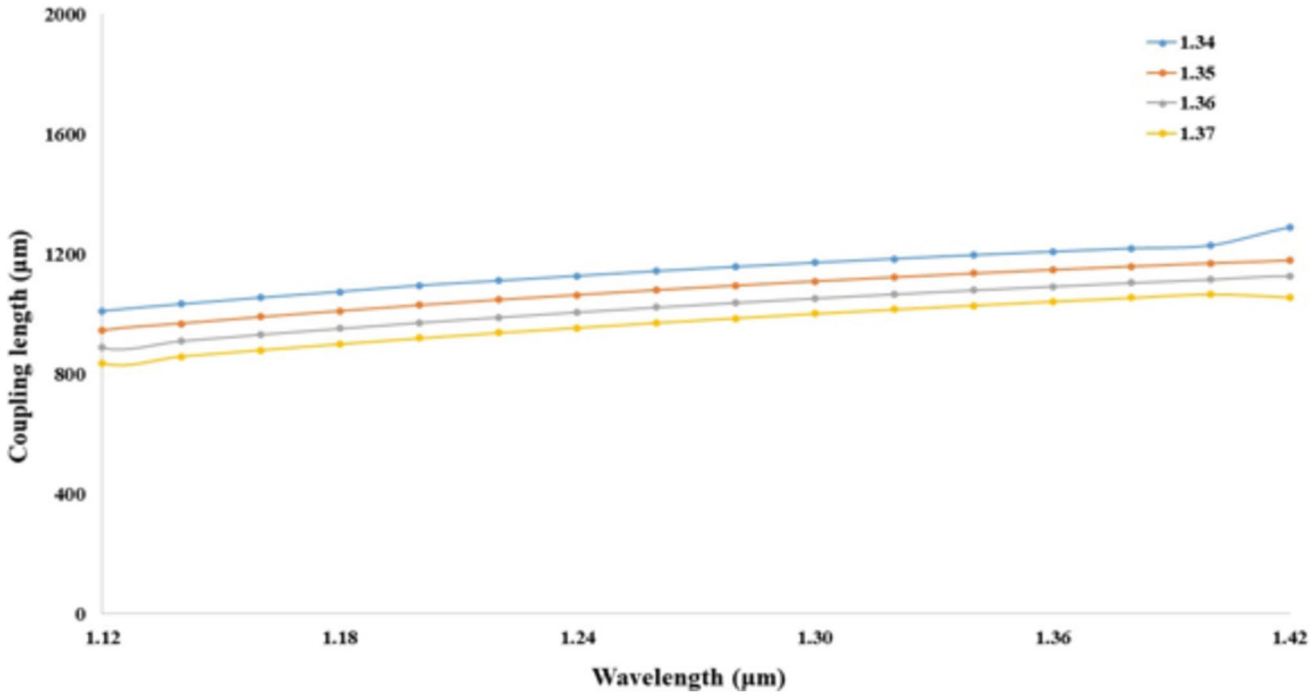

Fig. 6 Coupling length vs. wavelength curve

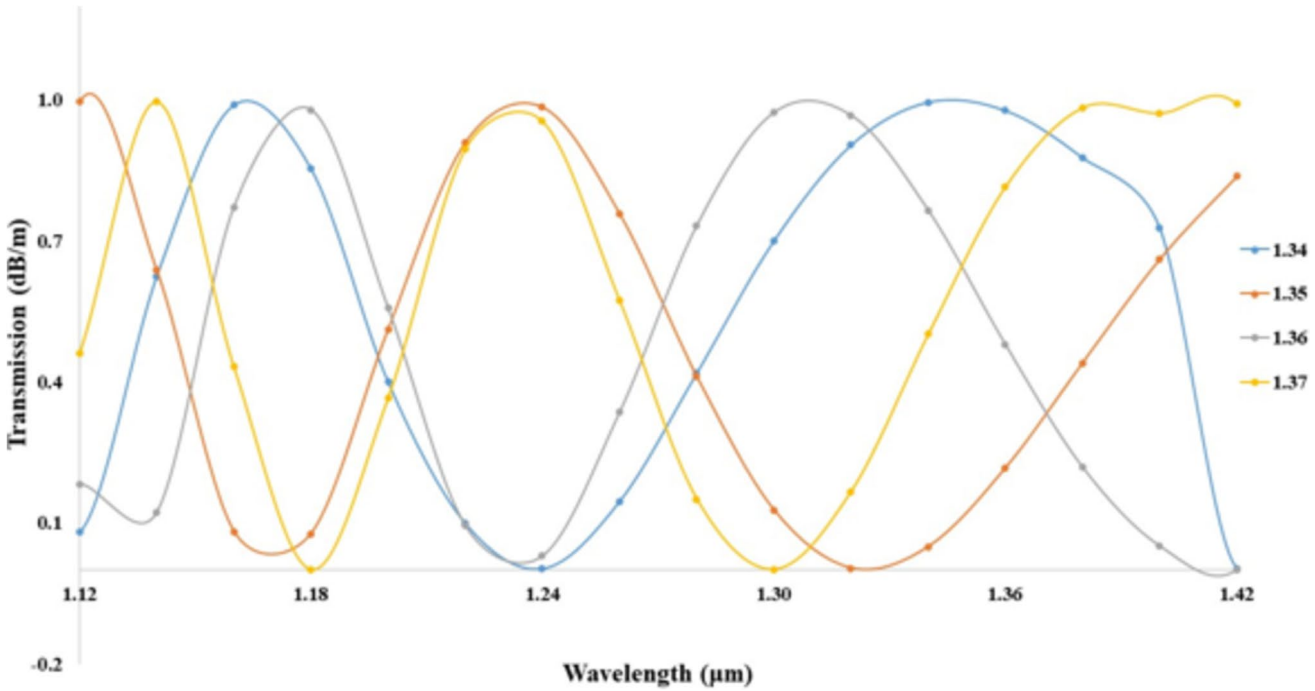

Fig. 7 Transmission spectrum vs. wavelength curve

conditions, where the phase-matching between the guided mode and the plasmonic mode results in energy transfer to the surface plasmon wave. These resonance dips are sensitive to changes in the RI of the surrounding medium, making the structure highly responsive to RI variations. Physically, the depth and position of the dips are governed

by the strength of the coupling and the plasmonic field's confinement at the metal–dielectric interface. A higher refractive index shifts the resonance wavelength, leading to changes in the TS. This behavior forms the basis for utilizing the structure in sensing applications, where precise monitoring of spectral shifts enables the detection of minute RI changes.

Figure 8 demonstrates the transmittance spectrum of the offered sensor for RI = 1.34–1.37. RI = 1.37 yields the highest transmittance of − 94 dB. The higher RI value had a denser profile compared to the lower RI value, which had a sudden downward peak. Consequently, greater analytes of $n = 1.37$ demonstrate two sudden downward peaks. However, the transmittance profile of RI = 1.34 was the most forward, whereas the result of RI = 1.37 was the most backward. In this manuscript, while a single peak is typically sufficient for single-parameter analysis, the inclusion of two peaks serves a distinct purpose. The first peak typically corresponds to the fundamental resonance mode, while the second peak may indicate the interaction of higher-order modes or additional resonance phenomena. The structure's optical behavior, including mode coupling, structural anisotropies, and the impact of different refractive index profiles, can be better understood owing to its dual-peak behavior. Additionally, two peaks can enhance sensing capabilities by providing multiple data points for measurement, improving the reliability and accuracy of the sensor.

In this manuscript, we designed a circular-shaped PCF-SPR sensor with a gold coating layer. The RI range of 1.34–1.37 is used to develop this sensor because this index range offers a balance of optimal light confinement, efficient plasmonic coupling, and compatibility with fabrication processes. This index range used in most of the articles [2, 22, 24, 26] ensures low optical losses and effective confinement of guided modes in the visible and near-infrared regions. This limited index range is important when the PCF is coated with gold because gold supports SPR and makes the fabrication process simpler. Besides, silica-based materials in this limited index range provide excellent mechanical stability, fabrication ease, and compatibility with existing IoT-based technologies. That is why in this experiment, we choose a limited RI range of 1.34–1.37, but in the future, we will expand the RI detection range for comparative analysis.

The comparative investigation of the suggested sensor and the prior sensors is shown in Table 1. On the basis of the operating wavelength with RI = 1.34–1.37, our offered sensor achieved a maximum WS (18,403.59 nm/RIU) and minimum loss peak (193.87 dB/cm), which indicates optimal results compared to the previously reported values. These optimal results suggest that we can employ this SPR-based sensor in the development of IoT-based devices.

An effective tool for remote, real-time, and extremely sensitive monitoring in a variety of domains is created by

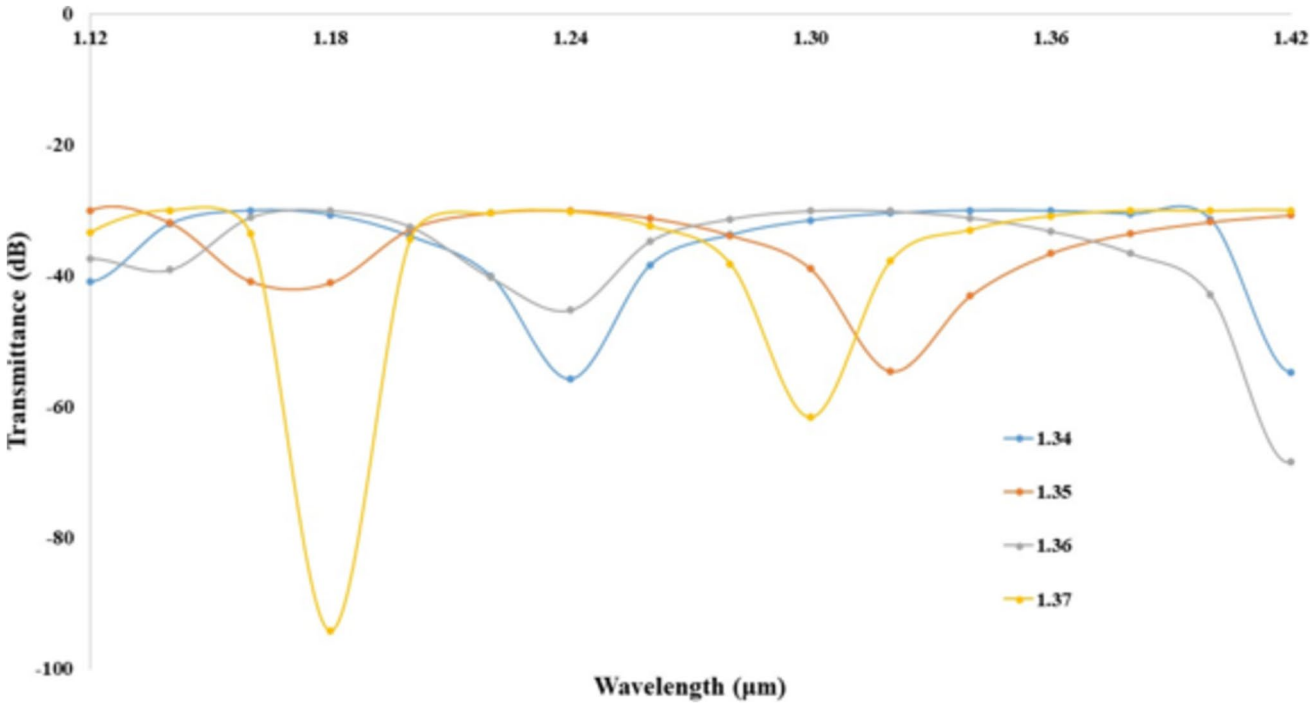

Fig. 8 Transmittance vs. wavelength curve

Table 1 Comparison table with prior works

Analyte range	Loss peak (dB/cm)	Maximum WS (nm/RIU)	Ref
1.34–1.37	700.05	9000	Mouvet et al. (1997) [2]
1.33–1.35	2500	2000	Dash et al. (2014) [22]
1.33–1.36	160	2200	Hasan et al. (2017) [26]
1.33–1.41	—	11,000	Azman et al. (2024) [27]
1.29–1.34	—	13,800	Sharif et al. (2023) [31]
1.33–1.37	600	5000	Dash et al. (2014) [24]
1.22–1.33	712.83	15,000	Liu et al. (2020) [37]
1.23–1.29	425	5500	Liu et al. (2017) [38]
1.46–1.485	695	2300	Rifat et al. (2016) [39]
1.36–1.39	449.91	6000	Hossen et al. (2018) [40]
1.423–1.523	—	12,500	Liao et al. (2020) [41]
1.20–1.40	—	21,000	Du et al. (2024) [42]
1.360–1.401	—	14,285.71	Ramola et al. (2021) [43]
1.31–1.40	—	12,100	Hossain et al. (2021) [44]
1.33–1.41	—	10,300	Wang et al. (2022) [45]
1.34–1.37	**193.87**	**18,403.59**	**Proposed**

combining IoT technology with SPR-based fiber optic sensors. The proposed sensor will provide scalable solutions for a range of applications, including environmental monitoring and healthcare, which will promote automation and data-driven decision-making in the existing IoT ecosystem. Besides, this proposed sensor can be applicable to make a quick decision by instant data collection and transfer to IoT platforms. The low power consumption of this sensor makes it more appropriate for Internet of Things (IoT) applications.

Conclusion

This manuscript analytically explores the propagating features of a remarkably sensitive SPR-based sensor for the development of sensing IoT centroid devices. A scattering threshold constraint is utilized to surround the analyte layer and gold (Au) layer in a two-layer SPR-based sensor. All the numerical parameters are optimized to get the highest AS (amplitude sensitivity) as well as the lowest CL (confinement loss). We achieve improved CL and AS by varying the diameter range, pitch parameter, PML layer, air hole, and chemical region amount. After tuning these parameters, the suggested configuration demonstrates a maximum WS (wavelength sensitivity) of 18,403.59 nm/RIU and 193.87 dB/cm, which is found to be the minimum peak loss of the structure. The suggested sensor is highly appropriate for developing IoT-based technologies. In the future, we will attempt to add various doping components to improve corresponding sensing abilities. We will try to modify the framework to boost the sensitivity of responses. The structure of the proposed sensor is very simple, so it would not be challenging to utilize in practice.

Acknowledgements The authors are grateful to the University Grants Commission of Bangladesh for their support in the research.

Author Contribution Mst Nargis Aktar: supervision, project administration, methodology, formal analysis, and conceptualization. Nilanjana Basak and Shuvo Biswas: writing—original draft, validation, resources, methodology, and conceptualization. Hasan Abdullah: software, resources, formal analysis, and conceptualization. Muhammad Shahin Uddin: writing—review and editing, visualization, validation, and investigation.

Funding This work was supported by the University Grants Commission of Bangladesh (grant ID: 37.01.0000.073.06.063.22.1870).

Data Availability No datasets were generated or analyzed during the current study.

Declarations

Ethics Approval Not applicable.

Consent to Participate Not applicable.

Consent to Publication.
Not applicable.

Competing Interests The authors declare no competing interests.

References

1. Chakma S, Khalek MA, Paul BK, Ahmed K, Hasan MR, Bahar AN (2018) Gold-coated photonic crystal fiber biosensor based on surface plasmon resonance: design and analysis. Sensing biosensing Res 18:7–12

2. Mouvet C, Harris RD, Maciag C, Luff BJ, Wilkinson JS, Piehler J, Brecht A, Gauglitz G, Abuknesha R, Ismail G (1997) Determination of simazine in water samples by waveguide surface plasmon resonance. Anal Chim Acta 338(1–2):109–117
3. Homola J (2003) Present and future of surface plasmon resonance biosensors. Anal Bioanal Chem 377:528–539
4. Otupiri R, Akowuah EK, Haxha S, Ademgil H, AbdelMalek F, Aggoun A (2014) A novel birefrigent photonic crystal fiber surface plasmon resonance biosensor. IEEE Photonics J 6(4):1–11
5. Akowuah EK, Gorman T, Ademgil H, Haxha S, Robinson GK, Oliver JV (2012) Numerical analysis of a photonic crystal fiber for biosensing applications. IEEE J Quantum Electron 48(11):1403–1410
6. Ortega-Mendoza JG, Padilla-Vivanco A, Toxqui-Quitl C, Zaca-Morán P, Villegas-Hernández D, Chávez F (2014) Optical fiber sensor based on localized surface plasmon resonance using silver nanoparticles photodeposited on the optical fiber end. Sensors 14(10):18701–18710
7. Rifat AA, Ahmed R, Yetisen AK, Butt H, Sabouri A, Mahdiraji GA, Yun SH, Adikan FM (2017) Photonic crystal fiber based plasmonic sensors. Sens Actuators, B Chem 243:311–325
8. Islam MS, Sultana J, Ahmed K, Islam MR, Dinovitser A, Ng BWH, Abbott D (2017) A novel approach for spectroscopic chemical identification using photonic crystal fiber in the terahertz regime. IEEE Sens J 18(2):575–582
9. Islam MI, Ahmed K, Asaduzzaman S, Paul BK, Bhuiyan T, Sen S, Islam MS, Chowdhury S (2017) Design of single mode spiral photonic crystal fiber for gas sensing applications. Sensing Bio-Sensing Res 13:55–62
10. Chowdhury S, Sen S, Ahmed K, Paul BK, Miah MBA, Asaduzzaman S, Islam MS, Islam MI (2017) Porous shaped photonic crystal fiber with strong confinement field in sensing applications: design and analysis. Sensing and Bio-Sensing Res 13:63–69
11. Sen S, Chowdhury S, Ahmed K, Asaduzzaman S (2017) Design of a porous cored hexagonal photonic crystal fiber based optical sensor with high relative sensitivity for lower operating wavelength. Photonic Sensors 7:55–65
12. Islam I, Paul BK, Ahmed K, Hasan R, Chowdhury S, Islam S, Sen S, Bahar AN, Asaduzzaman S (2017) Highly birefringent single mode spiral shape photonic crystal fiber based sensor for gas sensing applications. Sensing and bio-Sensing Res 14:30–38
13. Ahmed K, Morshed M (2016) Design and numerical analysis of microstructured-core octagonal photonic crystal fiber for sensing applications. Sensing Bio-Sensing Res 7:1–6
14. Paul BK, Ahmed K, Asaduzzaman S, Islam MS (2017) Folded cladding porous shaped photonic crystal fiber with high sensitivity in optical sensing applications: design and analysis. Sensing Bio-Sensing Res 12:36–42
15. Ritchie R (1957) Plasma losses by fast electrons in thin films. Phys Rev 106:874
16. Liedberg B, Nylander C, Lunström I (1983) Surface plasmon resonance for gas detection and biosensing. Sensors Actuators 4:299–304
17. Gupta BD, Verma RK (2009) Surface plasmon resonance-based fiber optic sensors: principle, probe designs, and some applications. J Sensors 2009(1):979761
18. Qin W, Li S, Yao Y, Xin X, Xue J (2014) Analyte-filled core self-calibration microstructured optical fiber based plasmonic sensor for detecting high refractive index aqueous analyte. Opt Lasers Eng 58:1–8
19. Wu Z, Chen X, Zhu S, Zhou Z, Yao Y, Quan W, Liu B (2012) Room temperature methane sensor based on graphene nanosheets/polyaniline nanocomposite thin film. IEEE Sens J 13(2):777–782
20. Maharana PK, Jha R (2012) Chalcogenide prism and graphene multilayer based surface plasmon resonance affinity biosensor for high performance. Sens Actuators, B Chem 169:161–166
21. Choi SH, Kim YL, Byun KM (2011) Graphene-on-silver substrates for sensitive surface plasmon resonance imaging biosensors. Opt Express 19(2):458–466
22. Dash JN, Jha R (2014) SPR biosensor based on polymer PCF coated with conducting metal oxide. IEEE Photonics Technol Lett 26(6):595–598
23. McPeak KM, Jayanti SV, Kress SJ, Meyer S, Iotti S, Rossinelli A, Norris DJ (2015) Plasmonic films can easily be better: rules and recipes. ACS Photonics 2(3):326–333
24. Dash JN, Jha R (2014) Graphene-based birefringent photonic crystal fiber sensor using surface plasmon resonance. IEEE Photonics Technol Lett 26(11):1092–1095
25. Yu X, Zhang Y, Pan S, Shum P, Yan M, Leviatan Y, Li C (2009) A selectively coated photonic crystal fiber based surface plasmon resonance sensor. J Opt 12(1):015005
26. Hasan MR, Akter S, Rifat AA, Rana S, Ali S (2017) A highly sensitive gold-coated photonic crystal fiber biosensor based on surface plasmon resonance. Photonics 4(1):18
27. Azman MF, Mashrafi M, Haider F, Ahmed R, Aoni RA, Junayed M, Ru WW, Mahdiraji GA, Adikan FRM (2024) Polarization selective PCF-based plasmonic biosensor for multi-analyte detection. Plasmonics 1–10
28. Mahfuz MA, Hossain MA, Haque E, Hai NH, Namihira Y, Ahmed F (2020) 'Dual-core photonic crystal fiber-based plasmonic RI sensor in the visible to near-IR operating band.' IEEE Sensors J 20(14):7692–7700
29. Srivastava R, Prajapati YK, Pal S, Kumar S (2022) 'Microchannel plasmon sensor based on a D-shaped photonic crystal fiber for malaria diagnosis with improved performance.' IEEE Sensors J 22(15):14834–14841
30. Haque E, Noman AA, Hossain MA, Hai NH, Namihira Y, Ahmed F (2021) 'Highly sensitive D-shaped plasmonic refractive index sensor for a broad range of refractive index detection.' IEEE Photon J 13(1):1–11
31. Sharif V, Pakarzadeh H (2023) 'High-performance surface plasmon resonance fiber sensor based on cylindrical vector modes.' Sci Rep 13(1):4563
32. Basak N, Sultana N, Mitu SA, Al-Zahrani FA, Patel SK, Ahmed K (2023) Exploration of LSPR-based refractive index sensor coated with silver-MgF2 layer. Plasmonics 18(1):271–282
33. Sakib MN, Hossain MB, Al-tabatabaie KF, Mehedi IM, Hasan MT, Hossain MA, Amiri IS (2019) High performance dual core D-shape PCF-SPR sensor modeling employing gold coat. Results in Physics 15:102788
34. Gauvreau B, Hassani A, Fehri MF, Kabashin A, Skorobogatiy M (2007) Photonic bandgap fiber-based surface plasmon resonance sensors. Opt Express 15(18):11413–11426
35. Ahmed K, AlZain MA, Abdullah H, Luo Y, Vigneswaran D, Faragallah OS, Eid MM, Rashed ANZ (2021) Highly sensitive twin resonance coupling refractive index sensor based on gold- and MgF2-coated nano metal films. Biosensors 11(4):104
36. Sun B, Chen MY, Zhang YK, Yang JC (2012) Design of refractive index sensors based on the wavelength-selective resonant coupling phenomenon in dual-core photonic crystal fibers. J Biomed Opt 17(3):037002–037002
37. Liu C, Wang J, Wang F, Su W, Yang L, Lv J, Fu G, Li X, Liu Q, Sun T, Chu PK (2020) Surface plasmon resonance (SPR) infrared sensor based on D-shape photonic crystal fibers with ITO coatings. Optics Communications 464:125496
38. Liu C, Yang L, Lu X, Liu Q, Wang F, Lv J, Sun T, Mu H, Chu PK (2017) Mid-infrared surface plasmon resonance sensor based on photonic crystal fibers. Opt Express 25(13):14227–14237

39. Rifat AA, Mahdiraji GA, Sua YM, Ahmed R, Shee YG, Adikan FM (2016) Highly sensitive multi-core flat fiber surface plasmon resonance refractive index sensor. Opt Express 24(3):2485–2495
40. Hossen MN, Ferdous M, Khalek MA, Chakma S, Paul BK, Ahmed K (2018) Design and analysis of biosensor based on surface plasmon resonance. Sensing and Bio-sensing Research 21:1–6
41. Liao J, Ding Z, Xie Y, Wang X, Zeng Z, Huang T (2020) Ultra-broadband and highly sensitive surface plasmon resonance sensor based on four-core photonic crystal fibers. Opt Fiber Technol 60:102316
42. Du Z, Liu H (2024) Elliptical photonic crystal fiber sensor for multi-function detection based on surface plasmon resonance. Indian J Phys 98(1):349–356
43. Ramola A, Marwaha A, Singh S (2021) Design and investigation of a dedicated PCF SPR biosensor for CANCER exposure employing external sensing. Appl Phys A 127(9):643
44. Hossain M, Sunny SAS, Ahmed T (2021) Design and analysis of circular lattice PCF biosensor-based on surface plasmon resonance. In: Proceedings of the 2021 3rd International Conference on Sustainable Technologies for Industry 4.0 (STI), Dhaka, Bangladesh, pp 1–4
45. Wang H, Chen S, Dai W, Cai X, Fu H (2022) A high sensitivity surface plasmon resonance biosensor based on photonic crystal fibers for refractive index sensing. In: Proceedings of the 2022 Photonics & Electromagnetics Research Symposium (PIERS), Hangzhou, China, pp 873–880